ResearchGate

See discussions, stats, and author profiles for this publication at: https://www.researchgate.net/publication/273178089

Impact of Anionic Br − Substitution on Open Circuit Voltage in Lead Free Perovskite (CsSnI 3−x Br x) Solar Cells

ARTICLE *in* THE JOURNAL OF PHYSICAL CHEMISTRY C · JANUARY 2015

Impact Factor: 4.77 · DOI: 10.1021/jp5126624

CITATIONS
2

READS
56

8 AUTHORS, INCLUDING:

Dharani Sabba
Nanyang Technological University
18 PUBLICATIONS **488** CITATIONS
SEE PROFILE

Hemant Kumar Mulmudi
Nanyang Technological University
19 PUBLICATIONS **413** CITATIONS
SEE PROFILE

Pablo P. Boix
Nanyang Technological University
59 PUBLICATIONS **1,879** CITATIONS
SEE PROFILE

Subodh G Mhaisalkar
Nanyang Technological University
383 PUBLICATIONS **8,421** CITATIONS
SEE PROFILE

Available from: Hemant Kumar Mulmudi
Retrieved on: 30 January 2016

THE JOURNAL OF PHYSICAL CHEMISTRY C

Article

pubs.acs.org/JPCC

Impact of Anionic Br^- Substitution on Open Circuit Voltage in Lead Free Perovskite ($CsSnI_{3-x}Br_x$) Solar Cells

Dharani Sabba,[†] Hemant Kumar Mulmudi,*[,†] Rajiv Ramanujam Prabhakar,[†] Thirumal Krishnamoorthy,[†] Tom Baikie,[†] Pablo P. Boix,[†] Subodh Mhaisalkar,[†,‡] and Nripan Mathews*[,†,‡]

[†]Energy Research Institute @NTU (ERI@N) Nanyang Technological University, Research Techno Plaza, Fifth Storey, 50 Nanyang Drive, Singapore, Singapore 637553

[‡]School of Materials Science and Technology, Nanyang Technological University, Block N4.1, Nanyang Avenue Singapore, Singapore 639798

Supporting Information

ABSTRACT: Replacement of lead in the hybrid organic−inorganic perovskite solar cells invokes the need for non-toxic materials such as Sn. Although solution processed $CsSnI_3$ has been demonstrated as a lead-free halide perovskite which can function as a light absorber with high photocurrent densities, the power conversion efficiencies were bottlenecked by low open circuit voltages. In this work, the open circuit voltages are modulated by chemical doping of $CsSnI_3$ with Br leading to formation of $CsSnI_{3-x}Br_x$ ($0 \le x \le 3$) perovskites. The beneficial effect of Br incorporation for V_{oc} improvement is evident for $CsSnI_3$ system even without the addition of SnF_2. There is an evolution of the crystal structure of $CsSnI_3$ from orthorhombic to cubic for $CsSnBr_3$ accompanied by changes in its optical properties with a blue shift of the absorption and IPCE onset, as the Br^- doping is increased. The V_{oc} enhancement is attributed to the decrease in Sn vacancies which is reflected by the lower charge carrier densities of 10^{15} cm^{-3} and a high resistance to charge recombination in case of Br rich $CsSnI_{3-x}Br_x$ perovskite. By the addition of SnF_2 to $CsSnI_{3-x}Br_x$ perovskite, the current densities are improved significantly.

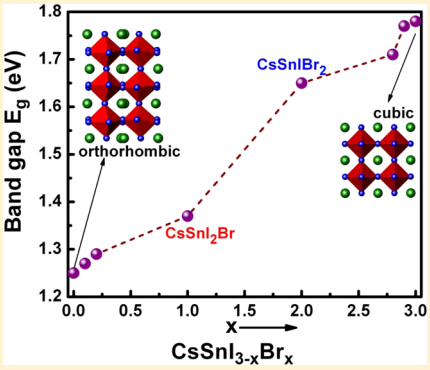

INTRODUCTION

The emergence of lead perovskite solar cells has had a major impact in the field of photovoltaic research as the power conversion efficiencies achieved until date are more than 19%.[1] These solar cells which are processed completely by solution-based methods make them amenable for low cost commercialization.[2−7] A key factor in making these solar cells commercially viable, are the efforts to replace toxic Pb with alternatives such as Sn.[8−10] High short-circuit current densities can be attained by Sn perovskites compared to the contemporary Pb-based perovskites owing to the small bandgap of Sn-based perovskites. However, attaining the otherwise theoretically deduced open circuit voltages by the tin-based perovskite has been limited by bulk recombination, attributable to high hole density caused by the decrease in the vacancies.[8,9] In our previous work, we showed that the charge carrier density (hole density) can be modulated by adding tin fluoride (SnF_2) which decreases the background charge carrier density (holes) in the system. In this manuscript, we investigate further the effect of substituting bromine in the lattice of $CsSnI_3$ in the absence as well as in the presence of SnF_2. A simple yet compelling method to tune the optical bandgap, carrier concentration and recombination in $CsSnI_3$ solar cells by bromine doping/substitution has been demonstrated. The high open circuit voltages derived by the widening of the band gap by Br doping/substitution is translated in terms of depreciating carrier concentration and increased resistance to charge recombination as revealed by impedance spectroscopy measurements.

RESULTS AND DISCUSSION

The thin film X-ray diffraction patterns for each of the synthesized perovskites are shown in Figure 1a (for ease of readability, only four compositions have been highlighted in the main text while the other compositions have been included in the Supporting Information). XRD analysis has been conducted for samples with and without the addition of SnF_2 (Figure S1, Supporting Information), and it is observed that with SnF_2, a pure $CsSnBr_3$ phase is attained (Figure 1a). This again demonstrates the beneficial effect of adding SnF_2 in the system. For $CsSnI_3$ the Bragg reflections were consistent with orthorhombic symmetry and the extracted lattice parameters (see Table S1) are in agreement with the values reported by Chung et al.[11] As the Br doping concentration was gradually increased as in case of $CsSnI_2Br$ (as well as for $CsSnI_{2.9}Br_{0.1}$ and $CsSnI_{2.8}Br_{0.2}$ in Table S1) a corresponding reduction in the lattice parameters/cell volume has been observed as the I^- (ionic radius =2.20 Å) is partially substituted with Br^- (ionic

Received: December 19, 2014
Revised: January 6, 2015
Published: January 6, 2015

ACS Publications © 2015 American Chemical Society

DOI: 10.1021/jp5126624
J. Phys. Chem. C 2015, 119, 1763−1767

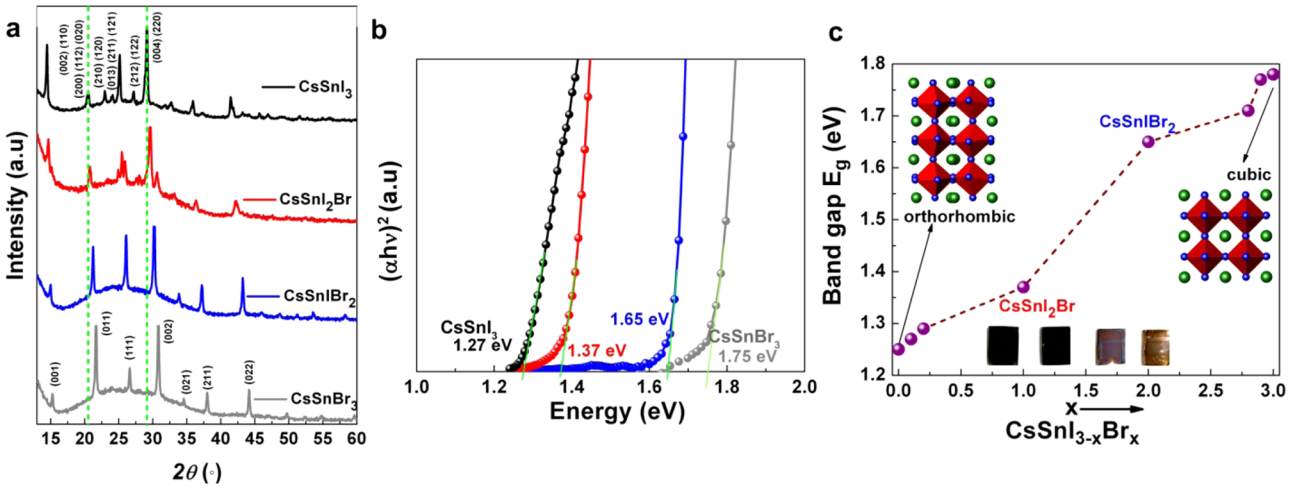

Figure 1. (a) XRD pattern for various compositions of $CsSnI_{3-x}Br_x$ ($0 \le x \le 3$) with 20 mol % SnF_2 addition. The crystal structure changes from orthorhombic for $CsSnI_3$ to cubic for $CsSnBr_3$. (b) Absorption spectroscopy of the films which show a blue shift upon inclusion of Br^- in the crystal structure of $CsSnI_3$. (c) Band gap variation with respect to Br^- concentration. The inset shows the photographs of samples: $CsSnI_3$, $CsSnI_2Br$, $CsSnIBr_2$ and $CsSnBr_3$ from left to right.

radius = 1.96 Å) indicating a successful incorporation of the smaller halogen in to the crystal lattice. For $CsSnIBr_2$ to $CsSnBr_3$, the Bragg reflections are in complete agreement with cubic symmetry and the variations in lattice parameters are consistent with the successful substitution of I^- with Br^-. For the stoichiometric compositions of $CsSnI_{0.2}Br_{2.8}$ and $CsSnI_{0.1}Br_{2.9}$ (see Figure S2) minor quantities of CsBr were also observed which are indicated by a (#).

Furthermore, the optical absorption spectra of the perovskite films with varying substitution of Br are shown in Figure 1b. The onset of optical bandgap edge transitions from 1.27 eV of $CsSnI_3$ to 1.37, 1.65, and 1.75 eV for $CsSnI_2Br$, $CsSnIBr_2$, and $CsSnBr_3$ respectively. This confirms that the inclusion of Br^- in the crystal lattice of $CsSnI_3$ is similar to the doping of Br^- in $CH_3NH_3PbI_3$, which led to an increment of the bandgap.[12−14] It is observed that the bandgap variation with respect to the composition of Br in $CsSnI_{3-x}Br_x$ is linear (with $R^2 = 0.98$) (shown in Figure 1c) which is coherent with Vegard's law,[15] implying that no anomalous behavior has been observed. From the inset of Figure 1c, it is apparent that as the substitution of Br^- increases, the color of the substrates gradually changed from black to dark brown and then to light brown which will reduce light harvesting while having a beneficial effect in increasing the open circuit voltage. Furthermore, from the plots of ln(absorption coefficient) with respect to photon energy (Figure S3), the Urbach energies (U_o) are deduced to be 16.8, 32, 39, and 32.6 meV for $CsSnI_3$, $CsSnI_2Br$, $CsSnIBr_2$, and $CsSnBr_3$ respectively.[16,17] These energies which are attributed to the inherent structural disorder of a material are low suggesting that these Sn-based perovskites have low structural disorders. The low U_o of $CsSnI_3$ is close to the U_o of $CH_3NH_3PbI_3$ as reported previously.[18] Also from Figure S3, it is evident that the absorption shoulder of $CsSnBr_3$ is lower than that of $CsSnI_3$, $CsSnI_2Br$. and $CsSnIBr_2$ which necessitates usage of thicker mesoporous TiO_2 films while fabricating solar cell. This trend is akin to that observed by Feng Ho et al. for $CH_3NH_3SnI_{3-x}Br_x$ perovskite.[8]

The bandgap tuning achieved by substitution of Br is anticipated to enhance the V_{oc} of $CsSnI_3$ perovskite without the addition of the reducing agent namely SnF_2. In order to validate this hypothesis, solid state photovoltaic devices have been fabricated with $CsSnI_3$ by varying the Br^- substitution in the absence of tin fluoride and the photovoltaic parameters have been tabulated in Table 1. From Table 1, it is evident that in the absence of SnF_2 the pure $CsSnI_3$ displayed negligible cell performance while the $CsSnBr_3$ samples exhibited considerable V_{oc} and FF clearly demonstrating the effect of Br in tailoring the electrical properties of the Sn-based perovskite. Interestingly, the V_{oc} of the $CsSnBr_3$ has plummeted, which could be attributed to the presence of an additional phase, $CsSn_2Br_5$ (Figure S1). This additional phase could be eliminated by adding SnF_2 to the perovskite precursor solution (Figure 1a). Similarly the low current densities can be ascribed to the high carrier densities due to presence of vacancies as was reported in our previous work.[9] This could be resolved by the

Table 1. Effect of Br^- Doping on the Photovoltaic Properties of the Solar Cells in the Absence and Presence of SnF_2 Reducing Agent[a]

sample details	V_{oc} (mV)	J_{sc} (mA/cm^2)	FF	η (%)	carrier density (cm^{-3})
$CsSnI_3$	2.30	0.22	0.57	3.02×10^{-4}	–
$CsSnI_3$: $CsSnBr_3$ (9:1)	120	0.49	0.25	0.002	–
$CsSnI_3$: $CsSnBr_3$ (1:1)	135	3.69	0.26	0.13	–
$CsSnI_3$: $CsSnBr_3$ (1:9)	227	1.32	0.41	0.12	–
$CsSnBr_3$	190	1.57	0.34	0.10	–
$CsSnI_3$ with SnF_2	201	27.67	0.29	1.66	5.28×10^{18}
$CsSnI_2Br$ with SnF_2	289	15.06	0.38	1.67	1.42×10^{17}
$CsSnIBr_2$ with SnF_2	311	11.57	0.43	1.56	6.32×10^{15}
$CsSnBr_3$ with SnF_2	410	3.99	0.58	0.95	–

[a]Variation of carrier density attained by Br^- doping has also been tabulated.

DOI: 10.1021/jp5126624
J. Phys. Chem. C 2015, 119, 1763−1767

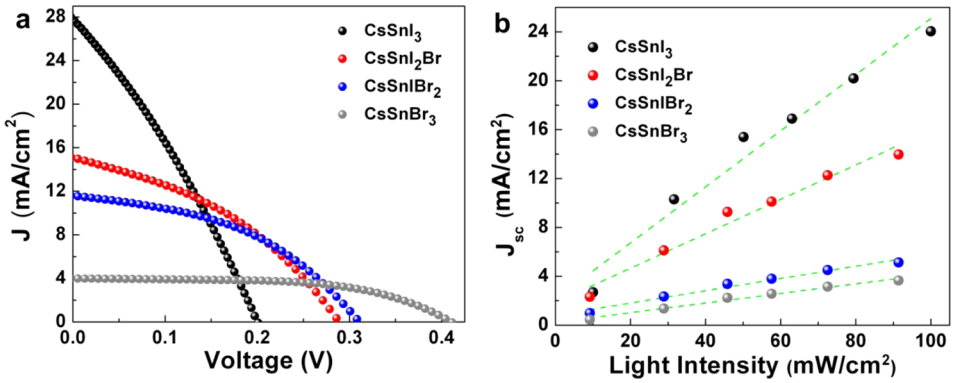

Figure 2. (a) $J-V$ graphs of different tin perovskite solar cells with concentrations varying from $CsSnI_{3-x}Br_x$ ($0 \leq x \leq 3$). The open circuit voltage increases as the Br_2 content increases in the films. (b) Light intensity effect on J_{sc} for various concentration of Br_2 doping of $CsSnI_3$.

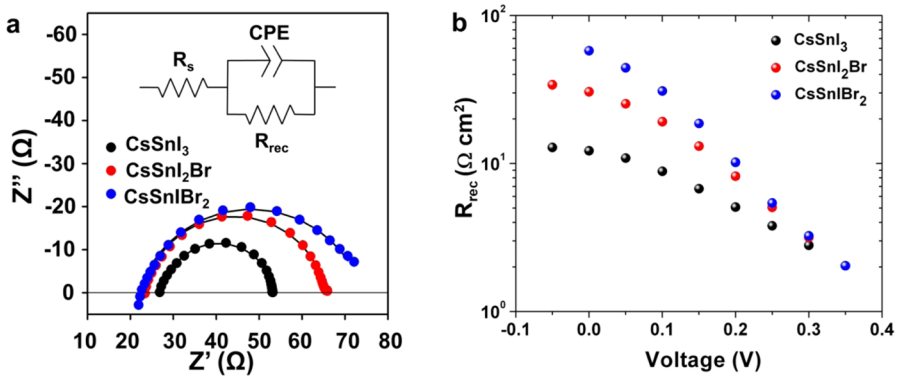

Figure 3. (a) Nyquist plots with the equivalent circuit in the inset and (b) recombination resistance vs applied voltage.

incorporation of SnF_2 (20 mol %) with the resultant photovoltaic parameters attained shown in Table 1 and Figure 2a.

Short-circuit photocurrent density (J_{sc}) of 27.67 mA/cm^2 under AM 1.5G solar illumination has been observed for $CsSnI_3$ (with SnF_2) solar cell, owing to the smaller band gap and better crystal quality attained by annealing the perovskite loaded TiO_2 films at 100 °C. The quality of the perovskite film is highly critical in affecting the cell performance as has been reported by other research groups and as such perovskite annealing temperatures are significant.[8] As reported in our previous work, $CsSnI_3$ covers the entire visible spectrum with an absorption onset at 976 nm, thereby contributing to high J_{sc} (22.7 mA/cm^2).[9] V_{oc} of 201 mV and a fill factor (FF) of 0.29, corresponding to a PCE of 1.66% (Figure 2a and Table 1) has been attained for pure $CsSnI_3$. As noted from the color transition from black to light brown for samples with increasing Br content the J_{sc} values depreciated from 27.67 mA/cm^2 to 15.06 mA/cm^2 for $CsSnI_2Br$, 11.57 mA/cm^2 for $CsSnIBr_2$ and 3.99 mA/cm^2 for $CsSnBr_3$ respectively. This trend is correlated to the blue shift of the absorption onset with increasing Br content in $CsSnI_3$ as is evident in the IPCE spectra of Figure S4. Coherent with the bandgap, the IPCE onset of $CsSnI_2Br$ is 900 nm while that of $CsSnIBr_2$ and $CsSnBr_3$ are 745 and 700 nm, respectively. Furthermore, by increasing the quantity of Br doping, there is a clear trend of escalating V_{oc} from 201 mV for $CsSnI_3$ to 410 mV for $CsSnBr_3$. In order to infer the origin of increasing V_{oc}, carrier density of $CsSnI_3$, $CsSnI_2Br$, and $CsSnIBr_2$ are estimated from the hall measurements and are shown in Table 1. From the hall measurements it is observed that $CsSnI_3$ is a p-type material with a high carrier density of 5.28×10^{18} cm^{-3} similar to the one reported in our previous work.[9] Doping of $CsSnI_3$ by Br has shown considerable reduction in its carrier density (Table 1). For $CsSnI_2Br$, the carrier density is reduced by 1 order of magnitude (1.42×10^{17} cm^{-3}) while for $CsSnIBr_2$ the reduction in carrier density is by almost 2 orders of magnitude (6.32×10^{15} cm^{-3}), clearly denoting a transition from metallic to semiconductor nature. $CsSnBr_3$ thin films were too resistive ($\rho > 10^5$ ohm.cm) to determine the carrier density. Thus, the combination of band gap increment and reduced background carrier density resulting in suppressing charge recombination with higher Br^- content lead to the attainment of higher V_{oc} (410 mV). This argument is further validated by the impedance spectroscopy (IS) analysis. The spectra obtained under AM 1.5 G illumination from 0 V to V_{oc} show a single arc as displayed in Figure 3a that can be fitted to the equivalent circuit consisting in a series and parallel resistances and a parallel capacitance (inset of Figure 3a). The parallel resistance, attributed to a recombination resistance (R_{rec}), increases for higher Br content (Figure 3b). Consequently, the R_{rec} of $CsSnIBr_2$ can explain the higher V_{oc} obtained for this sample regardless of its lower J_{sc}. Analogously, R_{rec} for $CsSnI_2Br$ and $CsSnI_3$ follow the same trend, with $CsSnI_3$ exhibiting lower R_{rec} (higher recombination rate) thereby yielding lower V_{oc} of the analyzed samples (201 mV).

Among the various compositions, $CsSnI_{2.9}Br_{0.1}$ yielded the best performance with a J_{sc} of 24.16 mA/cm^2, V_{oc} of 222 mV, and FF of 0.33 leading to a power conversion efficiency of 1.76% (Table S2). The increasing trend of FF for higher doping concentration of Br which is consistent with other works[8] is related to a thinner overlayer comprising only of the htm as is observed in the cross-sectional FESEM image of $CsSnBr_3$

DOI: 10.1021/jp5126624
J. Phys. Chem. C 2015, 119, 1763−1767

(Figure S5) in contrast to a thicker overlayer comprising of both the htm as well as the perovskite in case of $CsSnI_3$. Furthermore, the power conversion efficiency of $CsSnBr_3$ solar cell is improved to 1.28% (Table S3) by incorporating thicker TiO_2 scaffold. This demonstrates the possible channels to improve the cell performance of lead free perovskites in terms of high current densities accompanied by high open circuit voltages. From Figure 2b, it is worth noting that iodine rich samples exhibited nearly linear dependence of J_{sc} for various light intensities while the bromine rich cells demonstrated perfectly linear dependence of J_{sc}. This observation is correlated with the depreciation of the most common defects of $CsSnI_3$, such as Sn cation vacancies, which is also reflected in the lower charge carrier density measured by hall measurements. The nearly identical slopes calculated from the linear fitting of V_{oc} with respect to different light intensities (Figure S6) for $CsSnI_3$, $CsSnI_2Br$, $CsSnIBr_2$, and $CsSnBr_3$ reflects that the type of recombination is first order for all the $CsSnI_{3-x}Br_x$ perovskites in line with previous reports.[9,19] In $CH_3NH_3PbI_3$, it has been reported that substitution of Br^- improves the stability of the perovskite cell even at higher humidity levels (55%) due to the metamorphosis of crystal structure to cubic phase.[12,20] On the contrary the stability of $CsSnI_{3-x}Br_x$ is unaffected by Br^- substitution though the crystal structure of $CsSnBr_3$ attained is cubic. The primary chemical instability of $CsSnI_{3-x}Br_x$ is the tendency for Sn^{2+} ions to be converted to Sn^{4+}, which does not depend on the halide substitution- necessitating all the fabrication to be performed within the glovebox.[8,9]

CONCLUSION

In summary, this work demonstrates a viable method to increase the open circuit voltage of tin-based perovskite which is obtained by incorporation of Br anion in $CsSnI_{3-x}Br_x$. The crystal structure transforms from orthorhombic to cubic for $CsSnI_3$ to $CsSnBr_3$ respectively. The optical bandgap of the perovskite increases by 38.5% with a blue shift in the absorption spectra when I^- is progressively replaced by Br^-. Supplementing the increment in the bandgap, low charge carrier densities (6.32×10^{15} cm^{-3}) and increased charge recombination resistance aided in achieving high open circuit voltages of more than 400 mV. Addition of SnF_2 complemented by 100 °C post annealing of perovskite is found to be beneficial, contributing to the attainment of high photocurrent densities. The transition of nearly linear (for iodine rich) to perfectly linear (for bromine rich) dependence of short circuit current densities with respect to varying light intensities reflects the reduction of Sn cation vacancies by Br^- addition, which are the dominant defects in $CsSnI_3$. The recombination prevalent in all the $CsSnI_{3-x}Br_x$ perovskites is first order implying bimolecular recombination. The fill factors of Br rich perovskite solar cells are also higher than the iodine rich cells which are ascribed to the presence of negligible perovskite overlayer over the mesoporous TiO_2 film. The Urbach energies of these perovskites are small which are indicative of the low structural disorder inherent within them. This approach opens up new avenues for integrating lead free perovskites in applications where high photocurrents are mandatory.

EXPERIMENTAL SECTION

Physical and Electrical Characterization. Phase purity was confirmed by powder X-ray diffraction (PXRD) patterns collected with a Bruker D8 Advance diffractometer (Bragg–Brentano geometry) equipped with a Cu Kα X-ray tube operated at 40 kV and 40 mA using a step size of 0.02° and a time per step of 1 s. The thin-film samples were mounted in a Bruker air-sensitive sample holder and under these conditions; the intensity of the strongest reflection was approximately 2000 counts. Experimental fitting of the data was carried out from 10 to 50° 2θ using TOPAS V4.1.1 The lattice parameters of the $CsSnI_{3-x}Br_x$ perovskite were extracted via a Pawley fit and compared with the literature reported values.[11,21,22] XPS measurements were performed using a home-built system equipped with monochromatic Al K_α X-ray source and Omicron EA125 electron analyzer. Field Emission Scanning Electron Microscope (FESEM, JEOL, JSM-7600F, 5 kV) was used for recording top-view and cross-sectional images. For absorption measurements, soda lime glass substrates were coated with $CsSnI_{3-x}Br_x$ perovskite films and the absorption spectra were recorded by a UV–vis–NIR spectrophotometer (UV3600, Shimadzu) with 282 nm wavelength light source. The current voltage characteristics were measured using an Agilent 4155C analyzer and under AM 1.5G simulated illumination from a solar simulator (San-EI Electric, XEC-301S). The IPCE spectra were measured using a lock-in amplifier (Stanford Research Systems, SRS 810) with white light channeled from a Newport 300 W xenon lamp and through a 17 Hz mechanical chopper wheel and a monochromator (Oriel Cornerstone 130). No bias light was applied.

Electrical properties of $CsSnI_{3-x}Br_x$ films (carrier density and carrier mobility) were estimated using a MMR technologies variable temperature hall measurement system in a four-probe configuration. The $CsSnI_{3-x}Br_x$ films were spun coat on soda lime glass substrates (1 cm × 1 cm) and the hall measurements were carried out in vacuum (50 mTorr) at room temperature (302 K). Four square electrodes (1.6 mm × 1.6 mm) of gold were thermally evaporated in square geometry onto the $CsSnI_{3-x}Br_x$ films.

Impedance spectroscopy was measured with an Autolab PGSTAT302N. A 20 mV voltage perturbation was applied at different dc voltages ranging from 0 to V_{oc} with frequencies between 1 MHz and 1 Hz under 1 sun illumination. The results were fitted using the software Z-View.

Device Fabrication. A 60–70 nm blocking layer of TiO_2 was deposited onto cleaned, pre-etched fluorine doped tin oxide substrate by spray pyrolysis of titanium diisopropoxide bis(acetylacetonate) solution (75% in 2-propanol) diluted in ethanol (1:9 v/v). The substrates were subsequently treated in 0.1 M $TiCl_4$ solution for 60 min at 70 °C and were later annealed at 500 °C for 1–2 h. TiO_2 paste (DYESOL-30NRD) was diluted with ethanol in 2:7 w/w ratio and spin-coated onto the FTO substrate and sintered at 500 °C for 15 min. Deposition of perovskite, device fabrication and testing was done in nitrogen filled glovebox to prevent oxidation of Sn^{2+} to Sn^{4+}.

Solutions containing $CsSnI_{3-x}Br_x$ (0.6 M)(where x = 0, 0.1, 0.2, 1, 2, 2.8, 2.9, 3) + 20 mol % SnF_2 (Sigma-Aldrich, 99%) were stirred overnight at 70 °C in dimethyl sulfoxide (DMSO) by adding equimolar quantities of CsI/CsBr (Sigma-Aldrich, 99.9%) and $SnBr_2/SnI_2$ (Sigma-Aldrich, 99.99%) respectively. A 50 μL aliquot of this solution was used per substrate to spin coat on TiO_2 mesoporous substrates at 2000 rpm for 40 s. Prior to this step, the mesoporous films were subjected to ozone treatment at 100 °C for 10 min. After spin coating, the samples were annealed at 100 °C for 10 min. An organic hole conductor

DOI: 10.1021/jp5126624
J. Phys. Chem. C 2015, 119, 1763–1767

namely Spiro-OMeTAD (100 mg/mL chlorobenzene) was spin coated on these substrates. Additives like Li $(CF_3SO_2)_2N$ and *tert*-butylpyridine (TBP) were added to the above solution to improve conductivity. 80−100 nm thick Au electrodes were evaporated, defining an active area of 0.2 cm^2.

■ ASSOCIATED CONTENT

Supporting Information

Figures showing XRD patterns, FESEM images, Urbach energies extraction, IPCE spectra, and V_{oc} dependence on light intensities and tables listing lattice parameters and unit cell volumes for different doping concentrations of Br^- in $CsSnI_3$, photovoltaic parameters of $CsSnI_{3-x}Br_x$ ($1 \leq x \leq 3$), and effect of TiO_2 film thickness on the device performance. This material is available free of charge via the Internet at http://pubs.acs.org.

■ AUTHOR INFORMATION

Corresponding Authors

*E-mail: Nripan@ntu.edu.sg.

*E-mail: mulmudihk@ntu.edu.sg.

Notes

The authors declare no competing financial interest.

■ ACKNOWLEDGMENTS

Funding from National Research Foundation (NRF), Singapore, is acknowledged through CRP Award No.: NRF-CRP4-2008-03 and Singapore-Berkeley Research Initiative for Sustainable Energy (SinBeRISE) CREATE programme. N.M. acknowledges support from NTU Start-Up Grant M4081293 and the NTU-A*STAR Silicon Technologies Centre of Excellence under Program Grant No. 112 3510 0003.

■ REFERENCES

(1) Zhou, H.; Chen, Q.; Li, G.; Luo, S.; Song, T.-b.; Duan, H.-S.; Hong, Z.; You, J.; Liu, Y.; Yang, Y. Interface Engineering of Highly Efficient Perovskite Solar Cells. *Science* **2014**, *345*, 542−546.

(2) Kim, H.-S., et al., Lead Iodide Perovskite Sensitized All-Solid-State Submicron Thin Film Mesoscopic Solar Cell with Efficiency Exceeding 9%. *Sci. Rep.* **2012**, *2*.

(3) Xiao, M.; Huang, F.; Huang, W.; Dkhissi, Y.; Zhu, Y.; Etheridge, J.; Gray-Weale, A.; Bach, U.; Cheng, Y.-B.; Spiccia, L. A Fast Deposition-Crystallization Procedure for Highly Efficient Lead Iodide Perovskite Thin-Film Solar Cells. *Angew. Chem.* **2014**, *126*, 10056−10061.

(4) Jeon, N. J.; Noh, J. H.; Kim, Y. C.; Yang, W. S.; Ryu, S.; Seok, S. I. Solvent Engineering for High-Performance Inorganic−Organic Hybrid Perovskite Solar Cells. *Nat. Mater.* **2014**, *13*, 897−903.

(5) Xing, G.; Mathews, N.; Lim, S. S.; Yantara, N.; Liu, X.; Sabba, D.; Grätzel, M.; Mhaisalkar, S.; Sum, T. C. Low-Temperature Solution-Processed Wavelength-Tunable Perovskites for Lasing. *Nat. Mater.* **2014**, *13*, 476−480.

(6) Burschka, J.; Pellet, N.; Moon, S.-J.; Humphry-Baker, R.; Gao, P.; Nazeeruddin, M. K.; Gratzel, M. Sequential Deposition as a Route to High-Performance Perovskite-Sensitized Solar Cells. *Nature* **2013**, *499*, 316−319.

(7) Dharani, S.; Dewi, H. A.; Prabhakar, R. R.; Baikie, T.; Shi, C.; Yonghua, D.; Mathews, N.; Boix, P. P.; Mhaisalkar, S. G. Incorporation of Cl into Sequentially Deposited Lead Halide Perovskite Films for Highly Efficient Mesoporous Solar Cells. *Nanoscale* **2014**, *6*, 13854−13860.

(8) Hao, F.; Stoumpos, C. C.; Cao, D. H.; Chang, R. P. H.; Kanatzidis, M. G. Lead-Free Solid-State Organic-Inorganic Halide Perovskite Solar Cells. *Nat. Photon* **2014**, *8*, 489−494.

(9) Kumar, M. H.; et al. Lead-Free Halide Perovskite Solar Cells with High Photocurrents Realized through Vacancy Modulation. *Adv. Mater.* **2014**, *26*, 7122−7127.

(10) Noel, N. K.; et al. Lead-Free Organic-Inorganic Tin Halide Perovskites for Photovoltaic Applications. *Energy Environ. Sci.* **2014**, *7*, 3061−3068.

(11) Chung, I.; Song, J.-H.; Im, J.; Androulakis, J.; Malliakas, C. D.; Li, H.; Freeman, A. J.; Kenney, J. T.; Kanatzidis, M. G. $Cssni_3$: Semiconductor or Metal? High Electrical Conductivity and Strong near-Infrared Photoluminescence from a Single Material. High Hole Mobility and Phase-Transitions. *J. Am. Chem. Soc.* **2012**, *134*, 8579−8587.

(12) Noh, J. H.; Im, S. H.; Heo, J. H.; Mandal, T. N.; Seok, S. I. Chemical Management for Colorful, Efficient, and Stable Inorganic−Organic Hybrid Nanostructured Solar Cells. *Nano Lett.* **2013**, *13*, 1764−1769.

(13) Suarez, B.; Gonzalez-Pedro, V.; Ripolles, T. S.; Sanchez, R. S.; Otero, L.; Mora-Sero, I. Recombination Study of Combined Halides (Cl, Br, I) Perovskite Solar Cells. *J. Phys. Chem. Lett.* **2014**, *5*, 1628−1635.

(14) Kulkarni, S. A.; Baikie, T.; Boix, P. P.; Yantara, N.; Mathews, N.; Mhaisalkar, S. Band-Gap Tuning of Lead Halide Perovskites Using a Sequential Deposition Process. *J. Mater. Chem. A* **2014**, *2*, 9221−9225.

(15) Adachi, S. GaAs, AlAs, and $Al_xGa_{1-x}As$. *J. Appl. Phys.* **1985**, *58*, R1−R29.

(16) Urbach, F. The Long-Wavelength Edge of Photographic Sensitivity and of the Electronic Absorption of Solids. *Phys. Rev.* **1953**, *92*, 1324−1324.

(17) Ikhmayies, S. J.; Ahmad-Bitar, R. N. A Study of the Optical Bandgap Energy and Urbach Tail of Spray-Deposited Cds:In Thin Films. *J. Mater. Res. Technol.* **2013**, *2*, 221−227.

(18) De Wolf, S.; Holovsky, J.; Moon, S.-J.; Löper, P.; Niesen, B.; Ledinsky, M.; Haug, F.-J.; Yum, J.-H.; Ballif, C. Organometallic Halide Perovskites: Sharp Optical Absorption Edge and Its Relation to Photovoltaic Performance. *J. Phys. Chem. Lett.* **2014**, *5*, 1035−1039.

(19) Cowan, S. R.; Leong, W. L.; Banerji, N.; Dennler, G.; Heeger, A. J. Identifying a Threshold Impurity Level for Organic Solar Cells: Enhanced First-Order Recombination Via Well-Defined $Pc_{84}bm$ Traps in Organic Bulk Heterojunction Solar Cells. *Adv. Funct. Mater.* **2011**, *21*, 3083−3092.

(20) Lee, M. M.; Teuscher, J.; Miyasaka, T.; Murakami, T. N.; Snaith, H. J. Efficient Hybrid Solar Cells Based on Meso-Superstructured Organometal Halide Perovskites. *Science* **2012**, *338*, 643−647.

(21) Mori, M.; Saito, H. An X-Ray Study of Successive Phase Transitions in $Cssnbr_3$. *J. Phys. C: Solid State Phys.* **1986**, *19*, 2391.

(22) Scaife, D. E.; Weller, P. F.; Fisher, W. G. Crystal Preparation and Properties of Cesium Tin(Ii) Trihalides. *J. Solid State Chem.* **1974**, *9*, 308−314.

DOI: 10.1021/jp5126624
J. Phys. Chem. C 2015, 119, 1763−1767